Incommensurability and edge states in the one-dimensional $S=1$ bilinear-biquadratic model

Takahiro Murashima and Kiyohide Nomura
Department of Physics, Kyushu University, Fukuoka 812-8581, Japan
(Received 14 February 2006; revised manuscript received 2 May 2006; published 16 June 2006)

Commensurate-incommensurate change on the one-dimensional $S=1$ bilinear-biquadratic model $[\mathcal{H}(\alpha)=\Sigma_i\{\mathbf{S}_i\cdot\mathbf{S}_{i+1}+\alpha(\mathbf{S}_i\cdot\mathbf{S}_{i+1})^2\}]$ is examined. The gapped Haldane phase has two subphases (the commensurate Haldane subphase and the incommensurate Haldane subphase) and the commensurate-incommensurate change point (the Affleck-Kennedy-Lieb-Tasaki point, $\alpha=1/3$). There have been two different analytical predictions about the static structure factor in the neighborhood of this point. By using the Sørensen-Affleck prescription, these static structure factors are related to the Green functions, and also to the energy gap behaviors. Numerical calculations support one of the predictions. Accordingly, the commensurate-incommensurate change is recognized as a motion of a pair of poles in the complex plane.

DOI: 10.1103/PhysRevB.73.214431 PACS number(s): 75.10.Jm, 75.40.Mg, 73.43.Nq

I. INTRODUCTION

Commensurate-incommensurate (C-IC) transitions induced by frustration are important problems in many-body quantum spin systems. Among them, a C-IC change with an excitation gap is observed in one-dimensional (1D) quantum spin models.[1–3] This change is not a phase transition without an excitation gap. Whereas theories of C-IC transitions with no excitation gap (e.g., the Pokrovsky-Talapov transition[4]) have been developed, those of C-IC changes for quantum systems have not been yet. In some classical systems, analytical approaches to the C-IC change have been discussed,[5,6] and then a random phase approximation approach has been succeeded phenomenologically.[7] However, on the one hand the 1D frustrated Ising model for finite temperature cannot be mapped onto the 1D quantum case, on the other hand the transfer matrix for the 2D Ising model on the triangular lattice is nonsymmetric, thus its correspondence to the 1D quantum case is not a simple problem. Therefore independent analytical research for the 1D quantum C-IC change is needed.

There are typical quantum models which show the C-IC change; the 1D $S=1/2$ next-nearest-neighbor (NNN) model[1] and the 1D $S=1$ bilinear-biquadratic (BLBQ) model.[3] It is common between these models that the C-IC change occurs at the solvable point; the Majumdar-Ghosh point[8] in the 1D $S=1/2$ NNN model and the Affleck-Kennedy-Lieb-Tasaki (AKLT) point[9,10] in the 1D $S=1$ BLBQ model. These solvable points are called as the disordered point.[5,6] At the disordered point, the correlation length is the smallest and the ground state is described by the matrix product state.[8–10] The correlation length and the incommensurate wave number are not differentiable at the disordered point, although they are continuous. The structure factor (the Fourier transform of the correlation function) varies from the 2D Ornstein-Zernicke type (the modified Bessel function) in the commensurate and incommensurate regions to the 1D Ornstein-Zernicke type (the pure exponential function) at the disordered point.[11]

Recently, in order to explain the C-IC change, some analytical studies have been proposed. Fáth and Sütő have suggested that the C-IC change occurs because of the existence of higher derivatives in an effective Lagrangian of the 1D $S=1$ BLBQ model.[12] On the other hand, one of us (K.N.) has discussed the static structure factor.[13] These studies show two candidates for the static structure factor, although they do not necessarily decide between them.

By the way, Sørensen and Affleck (SA) have studied two spin correlations and energy gaps between the triplet and singlet states under the open boundary condition by means of field theoretic approaches,[14] although they have not considered the C-IC change. Applying the SA method to the C-IC problem, we can calculate some parameters included in the dynamical structure factor, i.e., the Green function. In our previous paper,[15] we have already found that the incommensurate wave number can be calculated by the energy gap of edge states. In this paper, we attempt to determine the Green function. After that, the relation between the singularities in the Green function and the incommensurability will be clear, and then we will obtain a unified view among commensurate and incommensurate behaviors.

In this stage, we summarize some known properties of the 1D $S=1$ BLBQ model with the Hamiltonian;

$$\mathcal{H}(\alpha)=\sum_i\{\mathbf{S}_i\cdot\mathbf{S}_{i+1}+\alpha(\mathbf{S}_i\cdot\mathbf{S}_{i+1})^2\}. \tag{1}$$

The ground state phase diagram of this model is shown in Fig. 1. This model is solvable at the AKLT point[9,10] $\alpha=\alpha_D=1/3$. The ground state is the valence-bond-solid (VBS) state with the lowest excitation gap at the mode $k=\pi$. One calls a phase, the ground state of which is a unique disordered ground state with a finite gap to the excited states, as the Haldane phase after Haldane's conjecture.[16] This phase extends from the Takhtajan-Bubujian (TB) point[17–19] $\alpha=-1$ to the Uimin-Lai-Sutherland (ULS) point[20–22] $\alpha=1$. At the TB or ULS points, the BLBQ model is also solvable, and has the gapless ground state with the soft mode $k=0,\pi$ or k

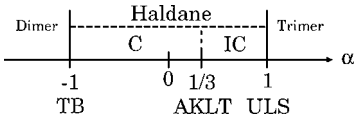

FIG. 1. Ground state phase diagram of the $S=1$ bilinear-biquadratic model.

$=0, \pm 2\pi/3$,[23] respectively. For $\alpha<-1$, there is the gapped dimerized (Dimer) phase,[9,24,25] whereas the gapless trimerized (Trimer) phase for $\alpha>1$.[25] Between the AKLT point and the TB point, the lowest excitation has the wave number $k=\pi$, while the lowest excitations have the incommensurate wave number k_{IC}, $2\pi/3<|k_{\mathrm{IC}}|\leqslant\pi$, between the AKLT point and the ULS point.[26] The wave numbers of the lowest excitations are different in these two regions, since the C-IC change occurs at the AKLT point.[3,11] The Haldane phase, therefore, has two subphases; the commensurate Haldane subphase for $-1<\alpha<1/3$ and the incommensurate Haldane subphase for $1/3<\alpha<1$.

In addition, the VBS state becomes increasingly significant in connection with quantum entanglements.[27–29] The entanglements have a close relation to the matrix product state as well as the C-IC change. Therefore it will be useful for an understanding of the quantum entanglements to investigate near the AKLT point, i.e., the C-IC change point.

The organization of this paper is as follows. In the next section, we summarize essential points of the static structure factor concerning the C-IC change. The analyticity of the static structure factor explains that the change between branch points and a pole in the static structure factor corresponds to the C-IC change. In Sec. III we discuss the relation between the edge states and the Green function on the basis of the SA prescription. From the analysis of this section and Sec. II, we expect some behaviors of the energy gap of edge states. Before we study the energy gap of edge states numerically, we discuss the lattice effect in Sec. IV. In Sec. V, we confirm the gap behavior of edge states numerically, which is related to the Kennedy degeneracy.[30] The last section gives a summary and a discussion.

II. STATIC STRUCTURE FACTOR AND INCOMMENSURABILITY

In our previous papers,[13,15] we have discussed the functional forms of the static structure factor concerning the C-IC change. Before studying the relation between edge states and the C-IC change, let us briefly summarize the essential points of the static structure factor about the C-IC change.

A. Analyticity of the static structure factor

From previous numerical results, especially in Ref. 11, one can find the static structure factor in each region as follows:

(1) In the commensurate region ($\alpha \ll \alpha_{\mathrm{D}}$),

$$S(q) \propto \frac{1}{\sqrt{q^2+m^2}}. \tag{2}$$

(2) At the disordered point ($\alpha=\alpha_{\mathrm{D}}$),

$$S(q) \propto \frac{1}{q^2+m^2}. \tag{3}$$

(3) In the incommensurate region ($\alpha \gg \alpha_{\mathrm{D}}$),

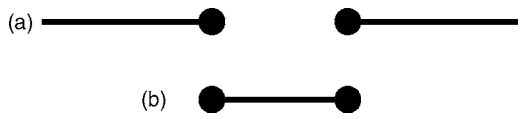

FIG. 2. Typical branch cuts of $f(z)=(z^2-d)^{-1/2}$. (a) $f(-z)=f(z)$. (b) $f(-z)=-f(z)$.

$$S(q) \propto \frac{1}{\sqrt{(q-q_{\mathrm{IC}})^2+m^2}} + \frac{1}{\sqrt{(q+q_{\mathrm{IC}})^2+m^2}}. \tag{4}$$

However, one cannot connect these three expressions continuously.

Considering an analytic continuation of real $S(q)$ to the complex plane, we can discuss $S(q)$ in the complex q plane. In terms of the singularity in the complex q plane, there are poles at the disordered point, in contrast to branch cuts in the other regions.

In order to unify these three expressions, we reconsider the relation between a pole and a branch cut. Considering the next function, we can transform a pole into a branch cut, and vice versa,

$$f(z) \equiv (z^2-d)^{-1/2}, \tag{5}$$

where d is a real parameter. This function has two branch points. Typical branch cuts of $f(z)$ are shown in Fig. 2. In the case of the branch cuts (a), which connect each of the branch points to infinite distance, $f(z)$ can be expanded in a Laurent series near $z=0$, and then $f(z)$ is found to be an even function $f(-z)=f(z)$. On the other hand, in the case of the branch cut (b) which connects both of the branch points, $f(z)$ is an odd function $f(-z)=-f(z)$ since $f(z)$ can be expanded at infinite distance (see Appendix A in detail). When $d=0$, a simple pole appears in case (b), whereas the branch cuts remain in case (a). Thus we select the branch cut (b), and then deal with $f(z)$ as an odd function.

Then we find $f(q-\tilde{m}i)$ satisfies

$$\overline{f(\bar{q}+\tilde{m}i)} = f(q-\tilde{m}i), \tag{6}$$

$$f[(-q)+\tilde{m}i] = -f(q-\tilde{m}i), \tag{7}$$

where $\tilde{m}$ is a real parameter. Note that q, $\bar{q}$, and $-q$ belong to the same Riemann sheet.

The static structure factor must satisfy several physical requirements (PRI):

(1) [reality on the real axis] $S(q)=\overline{S(\bar{q})}$.

(2) [parity] $S(q)=S(-q)$.

(3) [algebraic singularity] $S(q)$ is an analytic function of a complex variable q except for several algebraic singular points.

(4) [analyticity on the real axis] Singular points and branch cuts must not cross the real axis.

The above requirements represent properties of $S(q)$ on a fixed α. In addition,

(5) [α-dependency near α_{D}] $S(q)$ is an analytic function of a real parameter α in the neighborhood of α_{D}.

(6) [property at α_{D}] $S(q)$ is described with two simple poles at the disordered point.

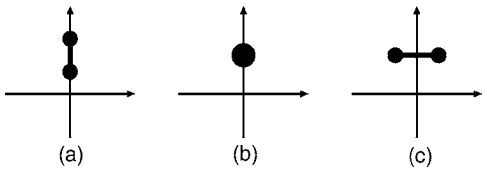

FIG. 3. Singularities of $f(q-\tilde{m}i)$ when (a) $d<0$, (b) $d=0$, and (c) $d>0$.

On the basis of these requirements, we can obtain two possible candidates of the static structure factor near the disordered point:

$$S_{\text{sing}}(q) = Af(q+\tilde{m}i)f(q-\tilde{m}i), \tag{8}$$

or

$$S_{\text{sing}}(q) = A\frac{i}{2\tilde{m}}[f(q+\tilde{m}i) - f(q-\tilde{m}i)], \tag{9}$$

where real parameters A, $\tilde{m}$, and d depend on α.[31] Figure 3 shows singularities of $f(q-\tilde{m}i)$ when (a) $d<0$, (b) $d=0$, and (c) $d>0$. $\tilde{m}$ represents a distance between the real axis and the center of two branch points. Equations (8) and (9) tend to $1/q^2$ at the $q\to\infty$ limit. The pre-factor $Ai/2\tilde{m}$ in the difference type function (9) is determined so that $S_{\text{sing}}(q)=A/(q^2+\tilde{m}^2)$ when $d=0$. Equation (8) is the same one which has first been proposed by Fáth and Sütő[12] and the other [Eq. (9)] is discussed by K.N.[13] We would like to clarify the behavior of the static structure factor $S(q)$ by using another approach. In the following sections, we will investigate which is a more appropriate structure factor, either Eq. (8) or (9).

B. α dependency

In addition, we can discuss how parameters $\tilde{m}$, d, and A depend on α. Since the correlation decays purely exponentially at the disordered point, we obtain $d=0$, $\tilde{m}>0$ at $\alpha=\alpha_{\text{D}}$. Generally, the requirement for the amplitude is $A\neq 0$ since the correlation function becomes perfectly zero for $A=0$. Near α_{D} we then expect that d, $\tilde{m}$, and A can be expanded in a Taylor series:

$$d = d_1(\alpha-\alpha_{\text{D}}) + d_2(\alpha-\alpha_{\text{D}})^2 + O((\alpha-\alpha_{\text{D}})^3), \tag{10}$$

$$\tilde{m} = \tilde{m}_0 + \tilde{m}_1(\alpha-\alpha_{\text{D}}) + O((\alpha-\alpha_{\text{D}})^2), \tag{11}$$

and

$$A = A_0 + A_1(\alpha-\alpha_{\text{D}}) + O((\alpha-\alpha_{\text{D}})^2). \tag{12}$$

Besides, PRI-4 in Sec. II A means that $\tilde{m}>\sqrt{-d}$ when $d<0$.

The incommensurate wave number $q_{\text{IC}}\equiv\sqrt{d}$, therefore, behaves as

$$q_{\text{IC}} = \sqrt{\alpha-\alpha_{\text{D}}}\sqrt{d_1+d_2(\alpha-\alpha_{\text{D}})} \tag{13}$$

in the incommensurate region, and $q_{\text{IC}}=0$ in the commensurate region. On the other hand, the correlation length ξ, which is related to the closest singular point to the real axis, behaves as

$$\xi^{-1} \propto \tilde{m} - \sqrt{-d} \tag{14}$$

in the commensurate region, and

$$\xi^{-1} \propto \tilde{m} \tag{15}$$

in the incommensurate region.

C. Numerical difficulties in dealing with the static structure factor

The previous consideration results in that the static structure factor should be Eq. (8) or (9). To select one from two possibilities, we may calculate numerically the correlation function with the DMRG method. However, there are some difficulties in dealing with the static structure factor directly. We require

(1) to calculate a long range correlation near the disordered point since the incommensurate wave number is small, although the correlation length is short,

(2) to consider how to avoid edge effects, and also,

(3) to improve accuracy in calculating the correlation function, since the correlation function is less accurate than the energy eigenvalues.

Though it is indirect, there is another approach which uses the energy eigenvalues under the open boundary condition (OBC). This method has high accuracy even near the disordered point. In addition, small size data are important since we need to investigate poles far from the real axis. We only need to relate the energy eigenvalues to the static structure factor.

In the next section, we will discuss the relation between the static structure factor and the energy eigenvalues under OBC, according to the SA prescription.[14]

III. EDGE STATES AND GREEN FUNCTION

In this section, we discuss a Green function based on the SA prescription[14] (see Appendix B in detail).

A. Modified SA prescription

Now we consider a Green function $G(q,\kappa)$ which is the Fourier transform of $G(x,\tau)$ in Euclidean space time. The Green function determines various physical quantities, which contain a static structure factor $S(q)$ and an energy gap of edge states. Between the Green function $G(q,\kappa)$ and a frequency ω_q (or an energy of a boson particle with a wave number q), the following relation is given in Appendix B:

$$G(q,\kappa) = \frac{1}{\kappa^2+\omega_q^2}, \tag{16}$$

where κ is an imaginary frequency. The static structure factor is obtained by applying the Fourier transform of $G(q,\kappa)$, and then limiting as $\tau\to 0$;

$$S(q) = \lim_{\tau\to 0}\int\frac{d\kappa}{2\pi}G(q,\kappa)e^{i\kappa\tau} = \frac{1}{2\omega_q}, \tag{17a}$$

which recalls the original relation. One can show the correlation function from the Fourier transform of the static structure factor.

$$\langle \mathbf{S}_x \cdot \mathbf{S}_y \rangle \equiv \int \frac{dq}{2\pi} e^{iq(x-y)} S(q). \tag{17b}$$

Next, we shall examine the relation between the Green function and edge states. The edge states mean the triplet states and the singlet state under OBC. Among these states, there is a energy difference:

$$\Delta E_{\mathrm{ST}} \equiv E_{\mathrm{triplet}} - E_{\mathrm{singlet}}. \tag{18}$$

The energy gap of edge states is connected with the Green function by the path integral method. The details are given in Appendix B. Here, we only show the relation between the energy gap of edge states and the Green function:

$$S_{\mathrm{eff}} = (-1)^L \lambda^2 \mathbf{S'}_1 \cdot \mathbf{S'}_L \int d\tau_1 d\tau_L \frac{d\kappa dq}{(2\pi)^2} G(q,\kappa) e^{iq(L-1)+i\kappa(\tau_L-\tau_1)}, \tag{19}$$

where the left-hand side of Eq. (19) means an effective action which is associated with an effective Hamiltonian, $S_{\mathrm{eff}} = \int d\tau \mathcal{H}_{\mathrm{eff}}$, and λ is an interaction parameter between the $S = 1/2$ edge spins $\mathbf{S'}_{1,L}$ and neighboring fields $\boldsymbol{\phi}$. The integral over τ_1 or τ_L provides a factor of $\delta(\kappa)$. Thus we obtain[32]

$$\Delta E_{\mathrm{ST}}(L-1) = (-1)^L \lambda^2 \int \frac{dq}{2\pi} G(q, \kappa = 0) e^{iq(L-1)}. \tag{20}$$

Comparing Eq. (17) with Eq. (20), we see that Eq. (20) is more manageable. The reason is that the integrand of Eq. (20), i.e., the Green function, has poles, while that of Eq. (17), i.e., the static structure factor, has branch points.

B. From static structure factor to Green function

In Sec. II, we have discussed the static structure factor. We can apply a similar discussion to the Green function. Corresponding to the static structure factor, the Green function is permitted to have the following functional forms:

$$G_{\mathrm{sing}}(q,\kappa) = \frac{1}{\kappa^2 + (2A)^{-2}[(q+\tilde{m}i)^2 - d][(q-\tilde{m}i)^2 - d]} \quad [\text{cf. Eq. (8)}] \tag{21}$$

or

$$G_{\mathrm{sing}}(q,\kappa) = G^{+}_{\mathrm{sing}}(q,\kappa) + G^{-}_{\mathrm{sing}}(q,\kappa) \quad [\text{cf. Eq. (9)}], \tag{22a}$$

where

$$G^{\pm}_{\mathrm{sing}}(q,\kappa) = \frac{1}{\kappa^2 - (A/\tilde{m})^{-2}[(q \mp \tilde{m}i)^2 - d]}. \tag{22b}$$

$G^{+}_{\mathrm{sing}}(q,\kappa)$ $[G^{-}_{\mathrm{sing}}(q,\kappa)]$ has the singularities only in the upper (lower) half q-plane. They satisfy

$$\overline{G^{\pm}_{\mathrm{sing}}(\bar{q},\bar{\kappa})} = G^{\mp}_{\mathrm{sing}}(q,\kappa), \tag{23a}$$

$$G^{\pm}_{\mathrm{sing}}(-q,\kappa) = G^{\mp}_{\mathrm{sing}}(q,\kappa), \tag{23b}$$

and

$$G^{\pm}_{\mathrm{sing}}(q,-\kappa) = G^{\pm}_{\mathrm{sing}}(q,\kappa). \tag{23c}$$

In Appendix C, we show that the static structure factor [Eq. (9)] is deduced from Eq. (22).

As well as the static structure factor, the Green function $G(q,\kappa)$ [both Eqs. (21) and (22)] must satisfy the following physical requirements (PRII):

(1) [reality on the real axes] $G(q,\kappa) = \overline{G(\bar{q},\bar{\kappa})}$.

(2) [parity] $G(q,\kappa) = G(-q,\kappa)$, $G(q,\kappa) = G(q,-\kappa)$.

(3) [algebraic singularity] $G(q,\kappa)$ is an analytic function of complex variables q and κ except for several poles.

(4) [analyticity on the real axes] Poles must not cross the real q and κ axes.

(5) [α-dependency near α_{D}] $G(q,\kappa)$ is an analytic function of a real parameter α in the neighborhood of α_{D}.

However, Eq. (21) is different from Eq. (22) when $d=0$ while the static structure factors [Eqs. (8) and (9)] are the same (cf. PRI-6 in Sec. II A). Another difference is that in the limit $q \to \infty$ Eq. (21) behaves as q^{-4} while Eq. (22) as q^{-2}. Hence it is easier to distinguish Eqs. (21) and (22) clearer than Eqs. (8) and (9) near the disordered point $\alpha = \alpha_{\mathrm{D}}$.

C. Energy gap of edge states

On the basis of the above discussion with Eq. (20), the energy gap of edge states obtained from Eq. (21) is

$$\begin{aligned}\Delta E_{\mathrm{ST}}(L-1) &= (-1)^L \lambda^2 \frac{A^2 e^{-\tilde{m}(L-1)}}{\tilde{m}\sqrt{d}\sqrt{\tilde{m}^2+d}} \times \sin[\sqrt{d}(L-1) + \phi(\tilde{m},d)] \\ &= (-1)^L \tilde{A} e^{-\tilde{m}(L-1)} \times \sin[\sqrt{d}(L-1) + \phi(\tilde{m},d)],\end{aligned} \tag{24a}$$

for $d>0$ (or $\alpha > \alpha_{\mathrm{D}}$), where $\phi(\tilde{m},d) = \tan^{-1}(\sqrt{d}/\tilde{m})$, and also

$$\begin{aligned}\Delta E_{\mathrm{ST}}(L-1) &= (-1)^L \lambda^2 \frac{A^2 e^{-\tilde{m}(L-1)}}{\tilde{m}\sqrt{-d}\sqrt{\tilde{m}^2+d}} \times \sinh[\sqrt{-d}(L-1) + \phi(\tilde{m},d)] \\ &= (-1)^L \tilde{A} e^{-\tilde{m}(L-1)} \times \sinh[\sqrt{-d}(L-1) + \phi(\tilde{m},d)],\end{aligned} \tag{24b}$$

for $d<0$ (or $\alpha < \alpha_{\mathrm{D}}$), where $\phi(\tilde{m},d) = \tanh^{-1}(\sqrt{-d}/\tilde{m})$.

On the other hand, the energy gap of edge states about Eq. (22) is

$$\begin{aligned}\Delta E_{\mathrm{ST}}(L-1) &= (-1)^L \lambda^2 \frac{A^2 e^{-\tilde{m}(L-1)}}{\tilde{m}^2\sqrt{d}} \sin[\sqrt{d}(L-1)] \\ &= (-1)^L \tilde{A} e^{-\tilde{m}(L-1)} \sin[\sqrt{d}(L-1)]\end{aligned} \tag{25a}$$

for $\alpha > \alpha_{\mathrm{D}}$, and also

$$\begin{aligned}\Delta E_{\mathrm{ST}}(L-1) &= (-1)^L \lambda^2 \frac{A^2 e^{-\tilde{m}(L-1)}}{\tilde{m}^2\sqrt{-d}} \sinh[\sqrt{-d}(L-1)] \\ &= (-1)^L \tilde{A} e^{-\tilde{m}(L-1)} \sinh[\sqrt{-d}(L-1)]\end{aligned} \tag{25b}$$

for $\alpha < \alpha_{\mathrm{D}}$.

We will verify which is more appropriate between these two predictions [Eqs. (24) and (25)] by analyzing numerical data in Sec. V. Note that Eq. (24) is apparently different from Eq. (25) when $L=1$: Eq. (25) is always equal to zero, whereas Eq. (24) is nonzero.

IV. IMPLEMENTATION FOR LATTICE

In this section, we consider an effect of the lattice structure. Equations (24) and (25) are not equal to zero even when L is not an integer number, and therefore they are incompatible with the lattice structure. To include the lattice structure, we must require $S(q)=S(q+2\pi)$ and $G(q,\kappa)=G(q+2\pi,\kappa)$.

Now, we organize the new physical requirements (PRIII) for the static structure factor and the Green function, considering the lattice structure. PRIII from 1 to 5 are the same as PRI and PRII. We add the requirement of the periodicity to PRIII:

(6) [periodicity] $S(q)=S(q+2\pi)$ and $G(q,\kappa)=G(q,\kappa+2\pi)$.

From PRIII-6, we derive another physical requirement:

(7) [singularity in the Brillouin zone] There are only four singular points (poles or algebraic singularity) in the first Brillouin zone ($-\pi<\mathrm{Re}\, q\leqslant\pi$).

All the information needed for any problem can be determined in this zone.

Then, we can construct some static structure factors and Green functions, satisfying these requirements, and we show them in Secs. IV A and IV B.

A. Infinite sum version

The easiest way is to consider the infinite sum of the translated singular parts. The static structure factor has the form as

$$S(q)=\sum_{j=-\infty}^{\infty} S_{\mathrm{sing}}(q+2\pi j)+S_{\mathrm{reg}}(q), \tag{26a}$$

and the Green function has

$$G(q,\kappa)=\sum_{j=-\infty}^{\infty} G_{\mathrm{sing}}(q+2\pi j,\kappa)+G_{\mathrm{reg}}(q,\kappa), \tag{26b}$$

where both $S_{\mathrm{sing}}(q+2\pi j)$ and $G_{\mathrm{sing}}(q+2\pi j)$ represent shifted singular terms. $S_{\mathrm{reg}}(q)$ and $G_{\mathrm{reg}}(q,\kappa)$ are regular functions in the whole q plane, such as

$$S_{\mathrm{reg}}(q)=\sum_{l=0}^{\infty} a_l\cos(lq), \tag{27}$$

where a_l is a real number. In Eq. (26), the singular terms correspond to long-range behaviors in the real space, whereas the regular terms correspond to model-dependent short-range behaviors.

Note that the infinite sum (26) for Eq. (2) or Eq. (4) is divergent, whereas that for Eq. (8) or Eq. (9) is convergent.

B. Sine wave version

Alternatively, substituting a 2π- or 4π-periodic function $p(q)$ for q in $S(q)$ or $G(q,\kappa)$, we also obtain a 2π-periodic static structure factor $S[p(q)]$ or a 2π-periodic Green function $G[p(q),\kappa]$, respectively. We impose some constraints on the periodic function $p(q)$ to satisfy PRIII:

(1) $p(q)$ is a holomorphic function.
(2) $p(q+2\pi)=p(q)$ or $p(q+2\pi)=-p(q)$.
(3) $p(-q)=p(q)$ or $p(-q)=-p(q)$.
(4) $\overline{p(\overline{q})}=p(q)$ or $\overline{p(\overline{q})}=-p(q)$.
(5) The inverse function $p(q)^{-1}$ is a single-valued function in the first Brillouin zone $-\pi<\mathrm{Re}\, q\leqslant\pi$.
(6) $\lim_{q\to 0} p(q)/q=1$.

The above requirements determine the distribution of zeros of $p(q)$. From Weierstrass' theorem for infinite products[33] and the above constraints, the function $p(q)$ is determined as

$$p(q)=2\sin\frac{q}{2}. \tag{28}$$

Replacing q in $S(q)$ and $G(q,\kappa)$ by $p(q)$, the static structure factor can be described as

$$S(q)=S_{\mathrm{sing}}[p(q)]+S_{\mathrm{reg}}(q), \tag{29a}$$

and the Green function as

$$G(q,\kappa)=G_{\mathrm{sing}}[p(q),\kappa]+G_{\mathrm{reg}}(q,\kappa). \tag{29b}$$

C. Contour

Corresponding to both the infinite sum version and the sine wave version, the contour C of the integral over q in Eqs. (17) and (20) is described in Fig. 4.

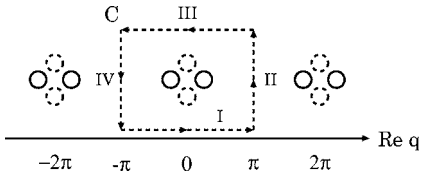

FIG. 4. Contour C for the integral over q in Eqs. (17) and (20).

Solid circles mean poles or branches for the incommensurate case, and broken circles for the commensurate case. I, II, III, and IV represent the contours

$\{q|(\mathrm{Re}\, q:-\pi\to\pi)\cap(\mathrm{Im}\, q=0)\}$,

$\{q|(\mathrm{Re}\, q=\pi)\cap(\mathrm{Im}\, q:0\to\infty)\}$,

$\{q|(\mathrm{Re}\, q:\pi\to-\pi)\cap(\mathrm{Im}\, q=\infty)\}$, and

$\{q|(\mathrm{Re}\, q=-\pi)\cap(\mathrm{Im}\, q:\infty\to 0)\}$, respectively.

The contributions of II and IV cancel each other out because of the periodicity. The contribution of III can be ignored since $S(q)$ and $G(q,\kappa)\lesssim q^{-2}$ as $q\to\infty$. We, therefore, obtain that $\oint_C=\int_I$. As a result, the integral of the infinite sum Green function [Eq. (26b)] is equal to Eqs. (24) and (25). A similar discussion can be applied to the static structure factor.

Note that the integral of the sine wave Green function [Eq. (29b)] is different from Eqs. (24) and (25). We consider it in detail in Appendix D.

V. NUMERICAL ANALYSIS

Our aim in this study is to decide between Eqs. (8) and (9). In the previous section, each behavior of the energy gap of edge states has been expected from Eqs. (8) or (9). In this section, we therefore carry out the numerical calculation of the energy gap between the triplet and singlet states, and verify whether the results correspond to the predictions [Eqs. (24) and (25)] with the use of a nonlinear least-squares (NLLS) fitting program, which needs appropriate initial values. Applying the previous results,[15] we guess the initial values first.

Although we have calculated the incommensurate wave number q_{IC} in Ref. 15, its analytical reasoning was unclear. Also, we have not so far investigated $\tilde{m}$ (the distance between the real axis and the center of two singular points) and $\tilde{A}$ (the amplitude of the energy gap). On the basis of the SA prescription, we will calculate them in this section. We will also trace the singularities in the commensurate region.

A. Surveys of edge states and incommensurability

We treat the $S=1$ BLBQ chain under OBC,

$$\mathcal{H} = \sum_{i=1}^{N} h_i, \tag{30a}$$

$$h_i = \mathbf{S}_i \cdot \mathbf{S}_{i+1} + \alpha(\mathbf{S}_i \cdot \mathbf{S}_{i+1}), \tag{30b}$$

where N is the number of the sub-Hamiltonian h_i and α is the interaction constant of the biquadratic term.

Note that $N=L-1$, where $L=\{6,7,\ldots,14\}$ is the chain length. We can treat longer chains ($L>14$). However, their significant digit is smaller than that of short chains ($L\leqslant 14$) since their amplitudes of the energy gap are exponentially small near the AKLT point. Thus we treat up to $L=14$. We exclude data smaller than $L=6$ since the short-range behaviors are affected by model-dependent regular terms, i.e., $S_{\mathrm{reg}}(q)$ and $G_{\mathrm{reg}}(q,\kappa)$ in Eqs. (26) and (29).

Since there are two edge $S=1/2$ spin freedoms at the AKLT point ($\alpha=\alpha_{\mathrm{D}}$), the following degeneracy occurs:

$$(S=1/2)\otimes(S=1/2)=(S=0)\oplus(S=1), \tag{31}$$

which reflects the $Z_2\times Z_2$ symmetry.[30,34–36] Therefore the singlet-triplet energy gap (or the gap of edge states)

$$\Delta E_{\mathrm{ST}}(N,\alpha) \equiv E_{\mathrm{triplet}}(N,\alpha) - E_{\mathrm{singlet}}(N,\alpha) \tag{32}$$

is zero for all length spin chains at the AKLT point:

$$\Delta E_{\mathrm{ST}}(N,\alpha_{\mathrm{D}}) = 0. \tag{33}$$

Note that in the thermodynamic limit the triplet states and the singlet state also become degenerate in the whole Haldane phase ($-1<\alpha<1$), and thus the amplitude of the gap of the edge states goes to zero as $N\to\infty$:

$$\lim_{N\to\infty} \Delta E_{\mathrm{ST}}(N,\alpha) = 0. \tag{34}$$

To avoid confusion, we call the degeneracy at the AKLT point as the AKLT degeneracy.

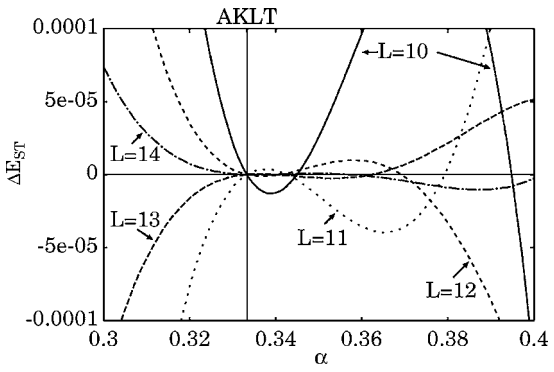

FIG. 5. Energy gaps of edge states $\Delta E_{\mathrm{ST}}=E_{\mathrm{triplet}}-E_{\mathrm{singlet}}$ as a function of α for various sizes.

Numerical results of the gap of edge states are shown in Fig. 5. For $\alpha\neq\alpha_{\mathrm{D}}$, the AKLT degeneracy breaks down. We see oscillating behaviors in the gap of edge states for $\alpha>\alpha_{\mathrm{D}}$. This phenomenon has been predicted from Eqs. (24a) and (25a). Note that for $\alpha<\alpha_{\mathrm{D}}$ the sign of the gap of edge states is different between even length chains and odd length chains because the parity of the bulk is different among these chains.[14]

B. Initial guess

1. Incommensurate wave number

Since the gap of edge states ΔE_{ST} is a function of α and N, and it is oscillating in the incommensurate phase, we can find the relation between α and N, taking account of the condition $\Delta E_{\mathrm{ST}}=0$. Then we consider the nth zero point of the singlet-triplet gap,

$$\Delta E_{\mathrm{ST}}[N,\alpha_n(N)] = 0. \tag{35}$$

If we adopt Eq. (25a), i.e., $\Delta E_{\mathrm{ST}}(N)\sim\sin(q_{\mathrm{IC}}N)$, in the incommensurate region, we can relate the incommensurate wave number q_{IC} with N as

$$q_{\mathrm{IC}}[\alpha_n(N)] = \frac{\pi n}{N}, \tag{36}$$

where $n=1,2,3,\ldots$. We have already found that they are fitted by a universal curve like $\sqrt{\alpha-\alpha_{\mathrm{D}}}$.[15] We show $q_{\mathrm{IC}}^2/(\alpha-\alpha_{\mathrm{D}})$ as a function of $\alpha-\alpha_{\mathrm{D}}$ in Fig. 6. These data fit well with the following equation:

$$d(\alpha) \equiv q_{\mathrm{IC}}^2 = d_1(\alpha-\alpha_{\mathrm{D}}) + d_2(\alpha-\alpha_{\mathrm{D}})^2 + O((\alpha-\alpha_{\mathrm{D}})^3), \tag{37}$$

where $d_1=11.230\pm0.010$ and $d_2=-65.76\pm0.83$.

If we adopt Eq. (24a), the corrections of $O(1/N)$ in d_1 and d_2 should be found. Since their corrections are smaller than 2%, we see that our guess adopting Eq. (25a), $\Delta E_{\mathrm{ST}}(N)\sim\sin(\sqrt{d}N)$, is more reliable than Eq. (24a). We expect that the gap of edge states behaves in the incommensurate and commensurate regions as Eqs. (25a) and (25b), respectively. This result means that the static structure factor is Eq. (9).

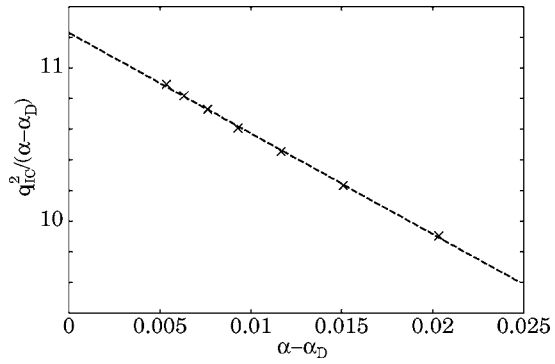

FIG. 6. Dependence of the incommensurate wave number q_{IC} on $\alpha-\alpha_D$.

In addition, the number of zero points n (except the AKLT point) and the system size $N(=\{1,\ldots,13\})$ are correlative. It is easy to find the following relation:

$$n \equiv N \pmod 3. \tag{38}$$

We see the relation between the max number of zero points $n^{\max}$ and N as

$$\frac{\pi n^{\max}(N)}{N} < \frac{\pi}{3}. \tag{39}$$

We can confirm this relation up to $N=13$ $[n^{\max}(13)=4]$. We expect that $\pi n^{\max}(N)/N$ has the limit $\pi/3$ as N tends to ∞, and therefore the position of the max-nth zero point $\alpha_{n^{\max}}$ goes to the ULS point as $N\to\infty$.

2. Amplitude and center of coupling poles

In the previous section we have found that the Green function corresponds to the difference type of the static structure factor [Eq. (9)]. Next, we examine the parameter $\tilde{A}$ and $\tilde{m}$.

In the incommensurate region $\alpha > \alpha_D$, we expect that the gap of edge states has the following form:

$$\Delta E_{ST}(N) = (-1)^{N+1}\tilde{A}e^{-\tilde{m}N}\sin(q_{IC}N). \tag{40}$$

The incommensurate wave number $q_{IC}(\alpha)$ near the AKLT point is obtained in the previous section. Using these values

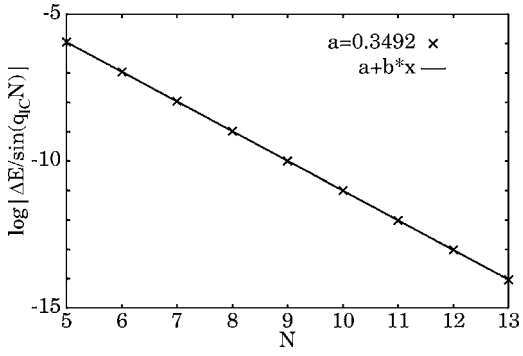

FIG. 7. Finite size results for $\log|\Delta E_{ST}/\sin(q_{IC}N)|$ when $\alpha=0.3492$.

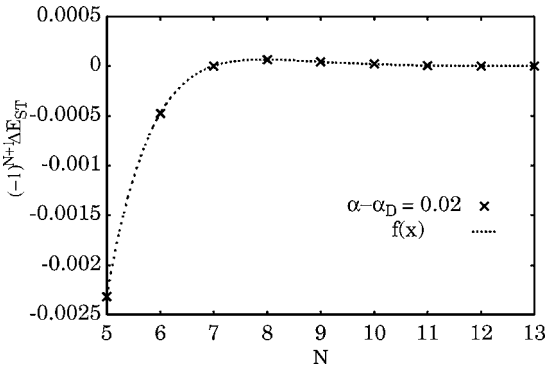

FIG. 8. Fitting results with Eq. (25) when $\alpha-\alpha_D=0.02$.

and considering the following equation, we can determine $\tilde{A}$ and $\tilde{m}$:

$$\log\left|\frac{\Delta E_{ST}(N)}{\sin(q_{IC}N)}\right| = \log|\tilde{A}| - \tilde{m}N. \tag{41}$$

Figure 7 shows $\log|\Delta E_{ST}/\sin(q_{IC}N)|$ when $\alpha=0.3492$ behaves linearly as a function of N. We have just confirmed our prediction for the incommensurate region.

Similar consideration can be applied to the commensurate region. In the region, the gap of edge states should be

$$\Delta E_{ST}(N) = (-1)^{N+1}\tilde{A}e^{-\tilde{m}N}\sinh(q_C N), \tag{42}$$

where $q_C=\sqrt{-d}=\sqrt{-(\alpha-\alpha_D)}\sqrt{d_1-d_2(\alpha-\alpha_D)}$. Here, the commensurate wave number q_C is indirectly determined by using d_1 and d_2, which are obtained from Eq. (37). Considering the following equation, we can obtain $\tilde{A}$ and $\tilde{m}$ in the commensurate region:

$$\log\left|\frac{\Delta E_{ST}(N)}{\sinh(q_C N)}\right| = \log|\tilde{A}| - \tilde{m}N. \tag{43}$$

C. Nonlinear least-squares fitting

In the previous section, we have adopted the commensurate wave number q_C indirectly determined by using the parameters of the incommensurate wave number in Eq. (37), although the relation between q_{IC} and q_C is somewhat unclear. Actually, it seems that the region, where Eq. (37) is

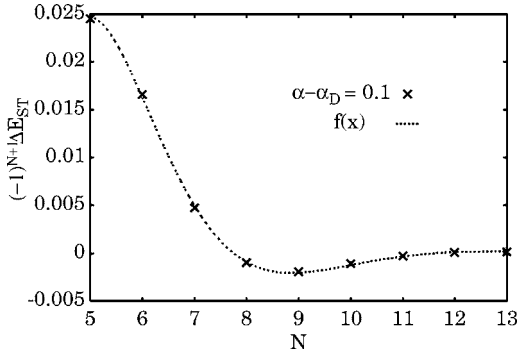

FIG. 9. Fitting results with Eq. (25) when $\alpha-\alpha_D=0.1$.

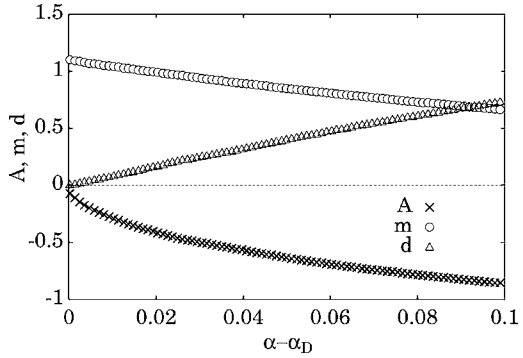

FIG. 10. Nonlinear least-squares fitting results with Eq. (25).

permitted, may be narrower in the commensurate side than in the incommensurate side. In order to check the above-mentioned results from another viewpoint, we employ a NLLS fitting method. Using this method, we can determine above parameters $\tilde{A}$, $\tilde{m}$, and d directly. Since the method requires appropriate initial values, we must have determined them in the previous section.

Taking into account the fact that the amplitude of the energy gap is exponentially small near the AKLT point, we use the following weighted values to perform the NLLS fitting program:

$$y_N = (-1)^{N+1}\Delta E_{\mathrm{ST}}(N) w_N, \tag{44}$$

where $w_N \equiv \exp(\tilde{m}' N)$ is a weight, and $\tilde{m}' = \tilde{m} + \delta$ is a value estimated from $\tilde{m}$ at the nearest α. Correctly, what we determine by the NLLS fitting method is not $\tilde{m}$ but δ.

The NLLS fitting method requires the minimization of the squared residuals,

$$Q = \sum_N \frac{1}{w_N^2}[y_N - f_N(\hat{\mathbf{x}})]^2, \tag{45}$$

where $\hat{\mathbf{x}} \equiv (\tilde{A}, \tilde{m}, d)$ and $f_N(\hat{\mathbf{x}})$ is a fitting function of $\hat{\mathbf{x}}$. From the minimum value of Q, we obtain parameters $(\tilde{A}, \tilde{m}, d)$.

In the case of $\alpha - \alpha_{\mathrm{D}} = 0.02$, for example, we show the data of the energy gap and the fitting function $f(\hat{\mathbf{x}}) = \tilde{A}\exp(-\tilde{m}N)\sin(\sqrt{d}N)$ where $\tilde{A} = -0.421$, $\tilde{m} = 0.991$, and $d = 0.202$ in Fig. 8. Also, the case of $\alpha - \alpha_{\mathrm{D}} = 0.1$ is shown in Fig. 9. The parameters of fitting function $f(\hat{\mathbf{x}})$ are $\tilde{A} = -0.758$, $\tilde{m} = 0.638$, and $d = 0.810$.

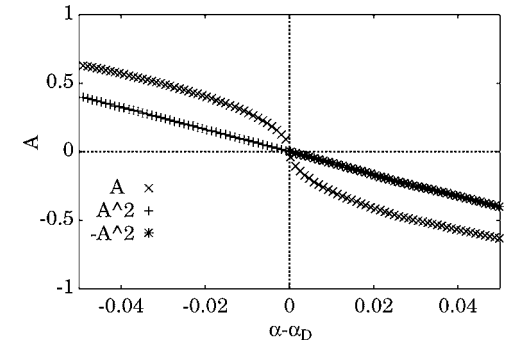

FIG. 11. Nonlinear least-squares fitting results for $\tilde{A}$.

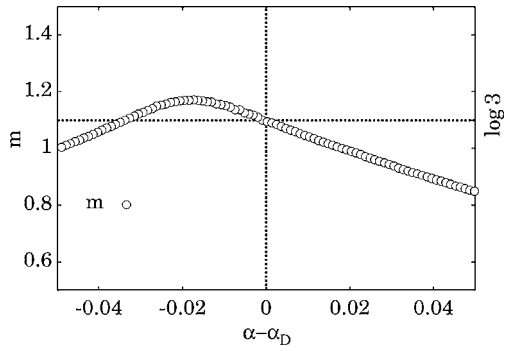

FIG. 12. Nonlinear least-squares fitting results for $\tilde{m}$.

1. Fitting with Eq. (25)

Figure 10 summarizes the fitting results with Eq. (25) in the incommensurate region. The obtained parameters, $\tilde{A}$, $\tilde{m}$, and d for $0 \leqslant |\alpha - \alpha_{\mathrm{D}}| \leqslant 0.05$, in which region Q is less than 1.0×10^{-8}, are shown in Figs. 11–13, respectively. Near the AKLT point, they converge very well, and behave continuously with α.

We see that these parameters are smooth between the commensurate and incommensurate regions. In Fig. 11, $\tilde{A}^2$ is highly linear. In Figs. 12 and 13 each parameter $\tilde{m}$, d varies linearly in the incommensurate region, whereas there are a broad maximum and a broad minimum, respectively, at $\alpha - \alpha_{\mathrm{D}} = -0.02$ in the commensurate region. The range where $d, \tilde{m}$, and A can be expanded in terms of $\alpha - \alpha_{\mathrm{D}}$ is narrower in the commensurate region than in the incommensurate region. When $\alpha - \alpha_{\mathrm{D}}$ is less than -0.02, there should be a different mechanism from what we have expected in Sec. II B, since PRIII-5 is not satisfied in the region.

Now, we estimate the correlation length ξ from the obtained data. Usually, the correlation length is related to an inverse of a distance between the closest singular point and the real axis. In the incommensurate region, $\xi = \tilde{m}^{-1}$, while $\xi = (\tilde{m} - \sqrt{-d})^{-1}$ in the commensurate region. These results are shown in Fig. 14. This behavior is consistent with the previous numerical result.[11]

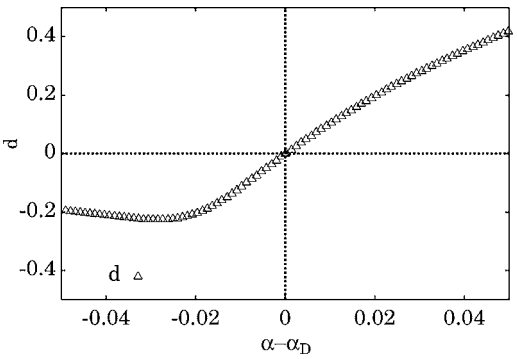

FIG. 13. Nonlinear least-squares fitting results for d.

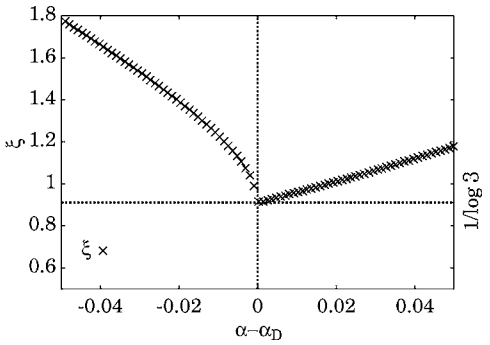

FIG. 14. Correlation length for $0 \leq |\alpha - \alpha_D| \leq 0.05$.

2. Fitting with Eq. (24)

We also attempt to apply the nonlinear least-squares fitting program to Eq. (24). The obtained parameters $(\tilde{A}, \tilde{m}, d)$ are shown in Fig. 15. We see that they behave as discontinuous pieces about α. In addition, the region where $d \propto \alpha - \alpha_D$ is very narrow. These facts mean that the supposed functions [Eqs. (8) and (24)] are not correct. Of course, the residual Q is larger than the one shown in the previous section.

3. About sine wave version

We have so far assumed the infinite sum version [Eq. (26)] as a lattice effect. Now we consider the case of the sine wave version [Eq. (29)]. The energy gap of edge states (in the incommensurate region) is modified as

$$\Delta E_{ST}(L-1) = (-1)^L \tilde{A} e^{\mathrm{Re}(\zeta)(L-1)} \times \sin[\mathrm{Im}(\zeta)(L-1)] \quad [\text{cf. Eq. (25a)}], \tag{46}$$

where $\zeta = -2\log(-iz + \sqrt{1-z^2})$ and $z = (\tilde{m}i + \sqrt{d})/2$ (see Appendix D). The obtained parameters with the NLLS fitting program are shown in Fig. 16. In this figure, the parameters behave continuously except for some discontinuous points near $\alpha - \alpha_D = 0.025$ and 0.065. Comparing Figs. 10 and 16, we think that the results of the infinite sum version [Eq. (26)] as a lattice effect are more reasonable than that of the sine wave version [Eq. (29)], although we have not found conclusive evidence to support it yet.

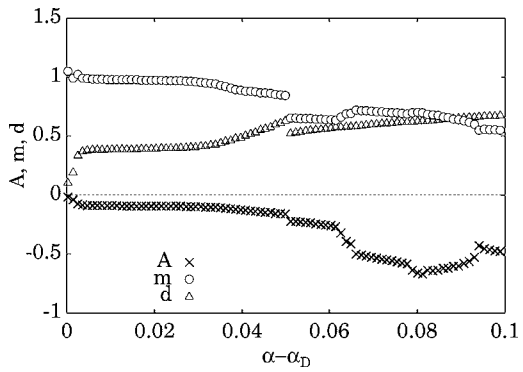

FIG. 15. Nonlinear least-squares fitting results with Eq. (24).

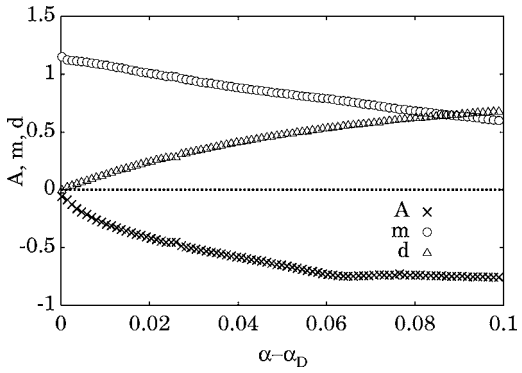

FIG. 16. Nonlinear least-squares fitting results with Eq. (46).

VI. SUMMARY AND DISCUSSION

In this study, we have examined the $S=1$ BLBQ model near the AKLT point. Analyzing the energy gap of edge states on the basis of the SA prescription,[14] we have shown that our numerical results support Eq. (25), i.e., Eq. (9) which is one of the predictions for the static structure factor concerned with the C-IC change. The energy gap of edge states is more manageable than the correlation function because the singularities are different among them, and thus our results are clearer than the previous one. We have also obtained the incommensurate wave number, the amplitude, and the correlation length. These results are consistent with the previous result.[11] Our incommensurate wave number q_{IC} is different from the original incommensurate wave number k_{IC} in Sec. I. The difference is caused by our notation; the prefactor $(-1)^{N+1}$ of the gap ΔE_{ST} is left apparently. Two different wave numbers can be related as $k_{IC} = \pi \pm q_{IC}$.

We should mention here that Eq. (25) is not only numerically supported, but also it has a physically favorable feature. From Eq. (25), one can see $\Delta E_{ST}(0) = 0$ for $L=1$, i.e., $N=0$ which means no sub-Hamiltonian case in Eq. (30). Although this property is not necessary since overall $G(q, \kappa)$ consists of singular and regular terms as Eqs. (26b) and (29b), the property $\Delta E_{ST}(0) = 0$ seems quite natural physically.

The amplitude $\tilde{A}$ has been found to be proportional to $\sqrt{\alpha - \alpha_D}$. This result implies that $\lambda^2 \propto \alpha - \alpha_D$ because of Eq. (25). In Appendix B and Ref. 14, we have only assumed that the interaction λ is some real constant. However, our results suggest that λ is some *complex* constant. Thus we have to modify the assumption for λ. Note that λ is equal to zero at the disordered point, corresponding to the VBS picture.

Originally in the SA prescription, the singlet-triplet energy gap ΔE_{ST} depends on the Green function, which is assumed to have a simple pole in the upper half-plane and in the lower half-plane. However, our results suggest that two poles should be concealed in the upper or lower half-plane. In general, one of these poles is far from the real axis, and therefore the ordinary field theoretic approach, like the nonlinear σ model,[16] appears to succeed in describing the Haldane phase. Indeed, if we explain the whole Haldane phase including the C-IC change, we must consider the four singular points. Near the AKLT point, a four-pole structure becomes explicit in the Green function, and then the incom-

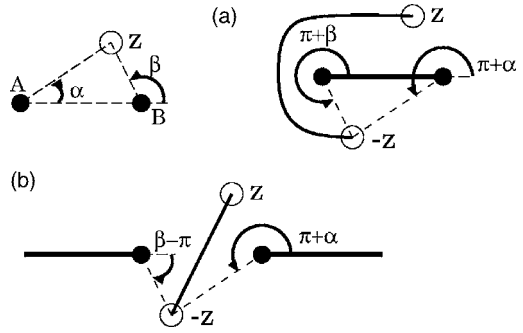

FIG. 17. Two typical types of branch cut of $f(z)=(z^2-d)^{-1/2}$. The points A and B show $z=-\sqrt{d}$ and $\sqrt{d}$, respectively.

mensurability occurs in the incommensurate Haldane subphase. A prelude to the incommensurability arises even in the commensurate region. We have found that positions of poles (singularities) included in the Green function are represented in terms of $(\tilde{m},d)$.

We have left some future tasks; the effective Lagrangian (maybe two components) and the dispersion curve for the Green function Eq. (22) [cf. those for Eq. (21) have been obtained in Ref. 12], and numerical verification of the static structure factor and the dynamical structure factor. Although we treat only the 1D $S=1$ BLBQ model in this paper, we have obtained similar results about the 1D $S=1/2$ NNN model.[15] However, we need to modify the discussion about the Green function since a quasiparticle has a magnonlike behavior in $S=1$ models, whereas a spinonlike behavior in $S=1/2$ models.

ACKNOWLEDGMENTS

The authors thank I. Affleck for introducing his paper[14] and fruitful discussions. K.N. thanks U. Schollwöck for encouragements and A. Sütő for giving a prompt to consider differences from his approach. The numerical calculation in this work is based on the program packages TITPACK version 2, developed by H. Nishimori. This research is partially supported by a Grant-in-Aid for Scientific Research (C), 18540376 (2006), from the Ministry of Education, Science, Sports and Culture of Japan.

APPENDIX A: DOUBLE-VALUED FUNCTION $f(z)$

In this appendix, we examine some properties of $f(z)$ [Eq. (5)] introduced in Sec. II A.

1. Choice of branch cuts and related property

The function

$$f(z)=(z^2-d)^{-1/2}=(z+\sqrt{d})^{-1/2}(z-\sqrt{d})^{-1/2} \tag{A1}$$

is a double-valued function with two branch points at $z=-\sqrt{d}$ and $z=\sqrt{d}$. We can freely choose branch cuts of $f(z)$ although the parity of the selected branch cut should be compatible with that of $f(z)$. Typical branch cuts are shown in Fig. 17: (a) both of the branch points are connected, and (b) each of them are connected to infinite distance. These different branch cuts bring different parities to $f(z)$.

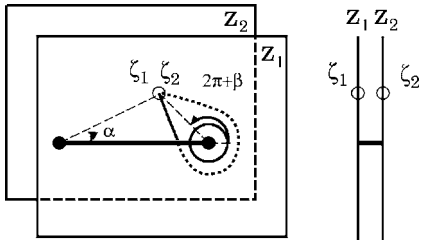

FIG. 18. Two Riemann sheets of $f(z)=(z^2-d)^{-1/2}$. ζ_1 is a point on the first sheet (z_1-plane), and ζ_2 is on the second sheet (z_2-plane).

We consider case (a) first. We can carry out the Laurent expansion of $f(z)$ around $z=\infty$ when $|z|>\sqrt{|d|}$:

$$(z^2-d)^{-1/2}=\frac{1}{z}\sum_{n=0}^{\infty}\frac{(2n-1)!!}{(2n)!!}\left(\frac{d}{z^2}\right)^n. \tag{A2}$$

It is an odd function with a zero point of order one at infinity.

About case (b), we can expand $f(z)$ around $z=0$ when $|z|<\sqrt{|d|}$, and then we obtain an even function:

$$(z^2-d)^{-1/2}=(-d)^{-1/2}\sum_{n=0}^{\infty}\frac{(2n-1)!!}{(2n)!!}\left(\frac{z^2}{d}\right)^n. \tag{A3}$$

Alternatively, we can explain their different parities by a graphical way. Let $z+\sqrt{d}=re^{i\alpha}$ and $z-\sqrt{d}=\rho e^{i\beta}$. Then

$$f(z)=r^{-1/2}\rho^{-1/2}e^{-i(\alpha+\beta)/2}. \tag{A4}$$

In case (a)

$$f(-z)=r^{-1/2}\rho^{-1/2}e^{-i(\pi+\beta+\pi+\alpha)/2}=-f(z), \tag{A5}$$

and in case (b)

$$f(-z)=r^{-1/2}\rho^{-1/2}e^{-i(\beta-\pi+\pi+\alpha)/2}=f(z). \tag{A6}$$

2. First and second sheets

The Riemann surface of $f(z)$ consists of two Riemann sheets. Here, we consider a relation between the first and second Riemann sheets (z_1- and z_2-plane, respectively), although we focus on the case that both branch points are connected by a branch cut. As shown in Fig. 18, let ζ_1 and ζ_2 be a point on the z_1- and z_2-plane, respectively, although these two points have the identical coordinate. A similar discussion in the previous section can be applied to the case of $\zeta_1\to\zeta_2$. Then we find

$$f(\zeta_2)=-f(\zeta_1). \tag{A7}$$

APPENDIX B: FIELD THEORETIC APPROACH FOR EDGE STATES

In this appendix we reproduce the Sørensen and Affleck prescription.[14] They start from the nonlinear σ (NLσ) model.[16] Since an effective field model is not clear in our case, it is not possible to apply this model as it is near the AKLT point. However, we can develop a similar discussion

if we assume a Green function $G(q,\kappa)$. The Green function is determined from discussions in Secs. II and III. It describes some massive free boson fields $\boldsymbol{\phi}(x,\tau)$:

$$\boldsymbol{\phi}(x,t) = \int \frac{dq}{\sqrt{2\pi}\sqrt{2\omega_q}}[\mathbf{a}(q)e^{iqx-i\omega_q t} + \mathbf{a}^\dagger(q)e^{-iqx+i\omega_q t}], \tag{B1}$$

where $\mathbf{a}(q)$ is a bose operator which satisfies $[\mathbf{a}(q),\mathbf{a}^\dagger(q')] = \delta(q-q')$, and ω_q is obtained from the Green function. Vacuum expectation values among two different boson fields are calculated as the following:

$$\langle \phi(x,t)\phi(0,0)\rangle = \int \frac{dq}{2\pi}\frac{e^{iqx-i\omega_q t}}{2\omega_q}. \tag{B2}$$

1. Static structure factor

Static structure factor $S(q)$ is defined as the Fourier transform of an equal-time correlation function:

$$\langle \phi(x,0)\phi(0,0)\rangle = \int \frac{dq}{2\pi}S(q)e^{iqx}. \tag{B3}$$

Therefore we can relate the static structure factor with ω_q:

$$S(q) = \frac{1}{2\omega_q}. \tag{B4}$$

2. Green function

Green function is defined as the time-ordered expectation value:

$$iG(x,t) = T\langle \phi(x,t)\phi(0,0)\rangle. \tag{B5}$$

Using the Wick rotation

$$t = -i\tau, \quad \omega = -i\kappa, \tag{B6}$$

where $\omega t = -\kappa\tau$, and the step function

$$\theta(\tau) = \frac{1}{2\pi}\int d\alpha \frac{e^{i\alpha\tau}}{i\alpha}, \tag{B7}$$

we then find

$$\begin{aligned}\int \frac{d\kappa dq}{(2\pi)^2}e^{iqx+i\kappa\tau}iG(q,\kappa) &= \int \frac{d\alpha dq}{2(2\pi)^2}\frac{1}{i\alpha\omega_q}(e^{iqx+i(-i\omega_q+\alpha)\tau} \\ &\quad + e^{-i(-i\omega_q+\alpha)\tau-iqx}) \\ &= \int \frac{d\kappa dq}{(2\pi)^2}e^{iqx+i\kappa\tau}\frac{i}{\kappa^2+\omega_q^2},\end{aligned} \tag{B8}$$

where κ is an imaginary frequency. The Green function $G(q,\kappa)$ associates with ω_q as

$$G(q,\kappa) = \frac{1}{\kappa^2+\omega_q^2}. \tag{B9}$$

3. Perturbation theory

Using the Green function $G(q,\kappa)$, we can describe a free part of the action.

$$S(\boldsymbol{\phi}) = \frac{1}{2}\int \frac{d\kappa dq}{(2\pi)^2}G^{-1}(q,\kappa)\tilde{\phi}^2 e^{iqx+i\kappa\tau}, \tag{B10}$$

where $\tilde{\phi}$ is the Fourier transform of $\boldsymbol{\phi}$.

Next, we take the edge effects into consideration. The open boundaries have the effect of leaving a $S=1/2$ degree of freedom at each end of the chain. The edge spins will interact with the rest of the system. To consider this effect, we assume the following interaction:

$$\mathcal{H}_1 = \lambda[\boldsymbol{\phi}(1)\cdot\mathbf{S'}_1 + (-1)^{L-1}\boldsymbol{\phi}(L)\cdot\mathbf{S'}_L], \tag{B11}$$

where λ is weak coupling constant. $\mathbf{S'}_1$ and $\mathbf{S'}_L$ are two $S=1/2$ excitations known to exist at the end of the open chain.[30,34–36] The sign in front of the second term comes from the reason that we consider the boson field ϕ with the wave number π.

Carrying out the ordinary Gaussian integral, we can obtain an effective action $S_{\text{eff}}(\mathbf{S'}_1,\mathbf{S'}_L)$.

$$\int \mathcal{D}\boldsymbol{\phi}e^{-S(\boldsymbol{\phi})+\int d\tau dx \mathbf{J}(x,\tau)\cdot\boldsymbol{\phi}(x,\tau)} = Ce^{-S_{\text{eff}}}, \tag{B12}$$

where $\mathbf{J}(x,\tau) = \lambda[\mathbf{S'}_1\delta(x-x_1) + (-1)^{L-1}\mathbf{S'}_L\delta(x-x_L)]$. Then we find

$$S_{\text{eff}} = (-1)^L\lambda^2\mathbf{S'}_1\cdot\mathbf{S'}_L\int d\tau_1 d\tau_L\frac{dqd\kappa}{(2\pi)^2}G(q,\kappa)e^{iq(L-1)+i\kappa(\tau_L-\tau_1)}. \tag{B13}$$

The constant C in Eq. (B12) contains the divergent *self-energy* that comes from terms with both arguments included in the Green function on the same source world-line. These correspond to virtual ϕ particles that are emitted and absorbed by the same source. We are not interested in these, but only in the variation in the vacuum energy as a function of the separation of the sources.

In this appendix, we have not considered an imaginary time dependency of $\mathbf{S'}_{1,L}$ since such a dependency has so far been unclear.

APPENDIX C: TRANSFORMATION FROM GREEN FUNCTION TO STATIC STRUCTURE FACTOR

In this appendix, we will show that the static structure factor [Eq. (9)] is constructed from the Green function [Eq. (22)].

We consider the following integral:

$$\int \frac{e^{i\kappa\tau}d\kappa}{(\kappa-\sqrt{z})(\kappa+\sqrt{z})} = \frac{i\pi e^{i\tau\sqrt{z}}}{\sqrt{z}}, \tag{C1}$$

where $\tau>0$, $z=re^{i\theta}$, and $\theta=\arg z$ $(0<\theta<2\pi)$. The right-hand side of Eq. (C1) is a double-valued function and has a branch point at $z=0$.

Now we consider $w=\sqrt{z}$. In general, w corresponds to $w_1=\sqrt{r}e^{i\theta/2}$ in the upper half w-plane when $0<\arg z<2\pi$, while w corresponds to $w_2=-\sqrt{r}e^{i\theta/2}$ in the lower half w-plane when $2\pi<\arg z<4\pi$. Thus Eq. (C1) is rewritten as

$$\int \frac{e^{i\kappa\tau}d\kappa}{(\kappa-\sqrt{z})(\kappa+\sqrt{z})} = \begin{cases} i\pi e^{i\tau w_1}/w_1 & (0 < \arg z < 2\pi), \\ i\pi e^{i\tau w_2}/w_2 & (2\pi < \arg z < 4\pi). \end{cases} \tag{C2}$$

Using Eq. (C2), we can show that

$$\lim_{\tau\to 0} \int \frac{d\kappa}{2\pi} e^{i\kappa\tau}[G_+(q,\kappa) + G_-(q,\kappa)] = A\frac{i}{2\tilde{m}}[f(q+\tilde{m}i) - f(q-\tilde{m}i)]. \tag{C3}$$

APPENDIX D: INTEGRATION OF GREEN FUNCTION ABOUT SINE WAVE VERSION

Substituting $p(q)=2\sin(q/2)$ for q in Eq. (22), we obtain the energy gap behavior of the edge states;

$$\Delta E_{\mathrm{ST}}(L-1) = (-1)^L \lambda^2 \frac{A^2}{\tilde{m}^2} \int \frac{dq}{2\pi} e^{iq(L-1)}\{G^+[p(q),\kappa] + G^-[p(q),\kappa]\}. \tag{D1}$$

Using the formula $\sin^{-1} z = i\log(-iz+\sqrt{1-z^2})$, we can integrate the right-hand side of Eq. (D1) over q. After the integration, we find

$$\Delta E_{\mathrm{ST}}(L-1) = (-1)^L \tilde{A} e^{\mathrm{Re}(\zeta)(L-1)} \sin[\mathrm{Im}(\zeta)(L-1)], \tag{D2}$$

where $\zeta=-2\log(-iz+\sqrt{1-z^2})$ and $z=(\tilde{m}i+\sqrt{d})/2$.

[1] T. Tonegawa and I. Harada, J. Phys. Soc. Jpn. **56**, 2153 (1987).
[2] T. Tonegawa, M. Kaburagi, N. Ichikawa, and I. Harada, J. Phys. Soc. Jpn. **61**, 2890 (1992).
[3] R. J. Bursill, T. Xiang, and G. A. Gehring, J. Phys. A **28**, 2109 (1995).
[4] V. L. Pokrovsky and A. L. Talapov, Sov. Phys. JETP **51**, 134 (1980).
[5] J. Stephenson, J. Math. Phys. **11**, 420 (1970).
[6] J. Stephenson, Phys. Rev. B **1**, 4405 (1970).
[7] T. Garel and J. M. Maillard, J. Phys. C **19**, L505 (1986).
[8] C. K. Majumdar and D. K. Ghosh, J. Math. Phys. **10**, 1388 (1969).
[9] I. Affleck, T. Kennedy, E. H. Lieb, and H. Tasaki, Phys. Rev. Lett. **59**, 799 (1987).
[10] I. Affleck, T. Kennedy, E. H. Lieb, and H. Tasaki, Commun. Math. Phys. **115**, 477 (1988).
[11] U. Schollwöck, T. Jolicoeur, and T. Garel, Phys. Rev. B **53**, 3304 (1996).
[12] G. Fáth and A. Sütö, Phys. Rev. B **62**, 3778 (2000).
[13] K. Nomura, J. Phys. Soc. Jpn. **72**, 476 (2003).
[14] E. S. Sørensen and I. Affleck, Phys. Rev. B **49**, 15771 (1994).
[15] K. Nomura and T. Murashima, J. Phys. Soc. Jpn. **74**, 42 (2005).
[16] F. D. M. Haldane, Phys. Lett. **93A**, 464 (1983).
[17] L. A. Takhtajan, Phys. Lett. **87A**, 479 (1982).
[18] H. M. Babujian, Phys. Lett. **90A**, 479 (1982).
[19] H. M. Babujian, Nucl. Phys. B **215**, 317 (1983).
[20] G. V. Uimin, JETP Lett. **12**, 225 (1970).
[21] C. K. Lai, J. Math. Phys. **15**, 1675 (1974).
[22] B. Sutherland, Phys. Rev. B **12**, 3795 (1975).
[23] G. Fáth and J. Sólyom, Phys. Rev. B **44**, 11836 (1991).
[24] J. Oitmaa, J. B. Parkinson, and J. C. Bonner, J. Phys. B **19**, L595 (1986).
[25] J. Sólyom, Phys. Rev. B **36**, 8642 (1987).
[26] O. Golinelli, T. Jolicœur, and E. Sørensen, Eur. Phys. J. B **11**, 199 (1998).
[27] F. Verstraete, M. A. Martín-Delgado, and J. I. Cirac, Phys. Rev. Lett. **92**, 087201 (2004).
[28] H. Fan, V. Korepin, and V. Roychowdhury, Phys. Rev. Lett. **93**, 227203 (2004).
[29] F. Verstraete and J. I. Cirac, Phys. Rev. A **70**, 060302(R) (2004).
[30] T. Kennedy, J. Phys.: Condens. Matter **2**, 5737 (1990).
[31] Previously (Ref. 13), K.N. has suggested a sum type of structure factor: $S_{\mathrm{sing}}(q)=\frac{A}{2q}[f(q+\tilde{m}i)+f(q-\tilde{m}i)]$. This structure factor has a simple pole at $q=0$ when $d\neq 0$, which does not satisfy PRI-4 in Sec. II. If we rewrite the sum type, it should have the following form: $S_{\mathrm{sing}}(q)=\frac{A}{f(q+\tilde{m}i)^{-1}+f(q-\tilde{m}i)^{-1}}[f(q+\tilde{m}i)+f(q-\tilde{m}i)] = Af(q+\tilde{m}i)f(q-\tilde{m}i)$, or the sum type is equal to the product type. Therefore we do not treat the sum type in this paper.
[32] We use the following relations: $\langle \mathrm{triplet}|\mathbf{S'}_1\cdot\mathbf{S'}_L|\mathrm{triplet}\rangle = 1/4$ and $\langle \mathrm{singlet}|\mathbf{S'}_1\cdot\mathbf{S'}_L|\mathrm{singlet}\rangle = -3/4$.
[33] L. V. Ahlfors, *Complex Analysis*, 3rd ed. (McGraw-Hill, New York, 1979), see Chap. 5.
[34] M. Hagiwara, K. Katsumata, I. Affleck, B. I. Halperin, and J. P. Renard, Phys. Rev. Lett. **65**, 3181 (1990).
[35] S. H. Glarum, S. Geschwind, K. M. Lee, M. L. Kaplan, and J. Michel, Phys. Rev. Lett. **67**, 1614 (1991).
[36] P. P. Mitra, B. I. Halperin, and I. Affleck, Phys. Rev. B **45**, 5299 (1992).